Journal of Alloys and Compounds 502 (2010) 5–12

Contents lists available at ScienceDirect

Journal of Alloys and Compounds

journal homepage: www.elsevier.com/locate/jallcom

In situ observation of the reaction of tantalum with nitrogen in a laser heated diamond anvil cell

Alexandra Friedrich[a,*], Björn Winkler[a], Lkhamsuren Bayarjargal[a], Erick A. Juarez Arellano[b], Wolfgang Morgenroth[a], Jasmin Biehler[a], Florian Schröder[a], Jinyuan Yan[c], Simon M. Clark[c]

[a] Institut für Geowissenschaften, Goethe-Universität Frankfurt, Altenhöferallee 1, D-60438 Frankfurt am Main, Germany
[b] Universidad del Papaloapan, Circuito Central 200, Parque Industrial, Tuxtepec 68301, Mexico
[c] Advanced Light Source, Lawrence Berkeley National Laboratory, MS6R2100, 1 Cyclotron Road, Berkeley, CA 94720-8226, USA

ARTICLE INFO

Article history:
Received 18 February 2010
Received in revised form 25 March 2010
Accepted 1 April 2010
Available online 24 April 2010

Keywords:
Tantalum nitride
Laser heating
Diamond anvil cell
High pressure
High temperature
Compressibility

ABSTRACT

Tantalum nitrides were formed by reaction of the elements at pressures between 9(1) and 12.7(5) GPa and temperatures >1600–2000 K in the laser-heated diamond anvil cell. The incorporation of small amount of nitrogen in the tantalum structure was identified as the first reaction product on weak laser irradiation. Subsequent laser heating led to the formation of hexagonal β-Ta_2N and orthorhombic η-Ta_2N_3, which was the stable phase at pressures up to 27 GPa and high temperatures. No evidence was found for the presence of ε-TaN, ϑ-TaN, δ-TaN, Ta_3N_5-I or Ta_3N_5-II, which was predicted to be the stable phase at $P > 17$ GPa and $T = 2800$ K, at the P, T-conditions of this experiment. The bulk modulus of η-Ta_2N_3 was determined to be $B_0 = 319(6)$ GPa from a 2nd order Birch–Murnaghan equation of state fit to the experimental data, while quantum mechanical calculations using the density functional theory gave a bulk modulus of $B_0 = 348.0(9)$ GPa for a 2nd-order fit or $B_0 = 339(1)$ GPa and $B' = 4.67(9)$ for a 3rd-order fit. The values show the large incompressibility of this high-pressure phase. From the DFT data the structural compression mechanism could be determined.

1. Introduction

Transition metal nitrides are chemically and structurally closely related to the binary transition metal carbides. The 'interstitial' nitrides of group IV and group V elements are refractory, they have high hardness and strength and often a high thermal conductivity [1]. This makes them interesting candidates for applications such as coatings and diffusion barriers in microelectronics, and this has driven research specifically for the understanding of tantalum nitrides. The present study complements earlier work by combined in situ experimental and theoretical investigations in order to provide further insight into the formation of tantalum nitrides.

A review of earlier work shows that there are several inconsistencies regarding the nomenclature of tantalum nitrides. For example, TaN in the WC structure has sometimes been designated as the δ-phase (e.g. [2]), while in other instances δ-TaN was used for the cubic phase with rock salt structure type [3]. In the following, the nomenclature used in Table 1 will be employed. There, the WC-structure (B_h) type TaN is designated ϑ-TaN, the cubic rock salt structure type TaN is called δ-TaN.

The ground state structure of TaN is of the CoSn-structure (B35) type. This polymorph, ε-TaN, is hexagonal (space group $P\bar{6}2m$) with $a = 5.196(4)$ Å and $c = 2.911(2)$ Å [4]. An earlier assignment of the space group $D^1_{6h} = P\frac{6}{m}$ mm or $D^1_6 = P622$ to the ε-phase [5,6] was erroneous.

There are at least two high pressure polymorphs of ε-TaN. Boiko and Popova [7] reported the synthesis of cubic ($Fm\bar{3}m$) δ-TaN in the range of 3–10 GPa at temperatures ≈ 2073 K when hexagonal ε-TaN was used as a starting material. At lower temperatures (T in the range of 673–2073 K) they obtained ϑ-TaN in the WC-structure type. However, no further experimental details are given. Heating cubic δ-TaN in vacuum leads to a transformation to ϑ-TaN in the WC-structure type [7]. This is consistent with experiments by Brauer et al. [8], who found the WC-structure type ϑ-TaN at high pressure syntheses in the pressure range of 2–10 GPa at 1073–1233 K. In all these experiments, the analyses of the products were done ex situ on quenched samples, and in all these studies the starting compound was ε-TaN. It was later shown [3] that δ-TaN could be produced from ε-TaN by heating at high temperatures (2273 K) under at least 0.001 GPa (10 bar) N_2-pressure. In that study [3] it was also noted that while ε-TaN is essentially stoichiometric, δ-TaN shows a compositional range, which influences the lattice parameter. Other synthesis routes for the production of δ-TaN have also been explored (for a brief review see Mashimo

* Corresponding author. Tel.: +49 (0)69 798 40114; fax: +49 (0)69 798 40109.
E-mail address: friedrich@kristall.uni-frankfurt.de (A. Friedrich).

0925-8388/$ – see front matter © 2010 Elsevier B.V. All rights reserved.
doi:10.1016/j.jallcom.2010.04.113

Table 1
Overview of stoichiometric tantalum nitrides. References: (1) Christensen and Lebech [4], (2) Brauer et al. [8], (3) Gatterer et al. [3], (4) Brauer and Zapp [5,6], (5) Fontbonne and Gilles [13], (6) Conroy and Christensen [14], Terao [2], (7) Zerr et al. [12], and (8) Strähle [15], Brese et al. [16]. Theoretical values are from the present study.

Phase	Symmetry	Lattice parameters		Comments	Reference
		Exp. [Å]	Theo. [Å]		
ε-TaN	$P\bar{6}2m$	$a = 5.196(4)$ $c = 2.911(2)$	$a = 5.261$ $c = 2.925$	CoSn-type(B35) Neutron diffraction	(1)
ϑ-TaN	$P\bar{6}m2$	$a = 2.936$ $c = 2.885$	$a = 2.949$ $c = 2.900$	WC-type (B_h) HP synthesis (2–10 GPa, 1073–1233 K)	(2)
δ-TaN	$Fm\bar{3}m$	$a = 4.331$	$a = 4.441$	NaCl-type (B1) HP synthesis (0.001–10 GPa, 2073–2273 K)	(3)
TaN	$P\frac{6}{m}mm$ or $P622$	$a = 5.1912$ $c = 2.9107$		Discredited in (1) Possibly ε-TaN ?	(4)
TaN	$P\frac{6_3}{m}mc$	$a = 3.048$ $c = 4.918$		Possibly Ta_2N ?	(5)
β-Ta_2N	$P\bar{3}1m$	$a = 5.285$ $c = 4.919$		With statistical occupation: $P6_3/mmc$, $a = 3.05$ Å	(6)
η-Ta_2N_3	$Pbnm$	$a = 8.191(2)$ $b = 8.183(2)$ $c = 2.9823(3)$	$a = 8.247$ $b = 8.308$ $c = 3.012$	HP synthesis from Ta_3N_5 (11–20 GPa, 1773–1973 K)	(7)
Ta_3N_5	$Cmcm$	$a = 3.890$ $b = 10.26$ $c = 10.26$	$a = 3.979$ $b = 10.415$ $c = 10.392$	16 K neutron powder diffraction	(8)
Ta_4N_5	$I\frac{4}{m}$	$a = 6.831$ $c = 4.269$			(5)
Ta_5N_6	$P\frac{6_3}{m}cm$	$a = 5.176$ $c = 10.353$			(5)

et al. [9]), including 'rapid solid state metathesis', which gives a mixture of δ-TaN ($a = 4.32$ Å) and a hexagonal phase [10], or ion irradiation [11]. Recently, a novel high-pressure phase of tantalum nitride, orthorhombic η-Ta_2N_3, was synthesized using Ta_3N_5 as starting product and a multi-anvil apparatus in order to generate pressures between 11 and 20 GPa and temperatures between 1773 and 1973 K [12]. A high Vickers hardness of at least $H_v(0.5) = 16$ GPa was attributed to this phase.

A number of theoretical studies have addressed the stability of tantalum nitrides. Stampfl and Freeman [17] studied the stability of a range of compounds based on a computed chemical potential, but did not investigate the stability of phases as a function of pressure. For Ta_2N they seem to have studied the unit cell proposed for space group $P6_3/mmc$ with $a = 3.05$ Å and $c = 4.92$ Å [2]. However, in a hexagonal cell with this space group, the occupation of Wyckoff position 0,0,0 by a nitrogen atom implies a symmetrically equivalent atom on 0,0,$\frac{1}{2}$—and for model calculations, in which all positions are fully occupied, the stoichiometry would be Ta_2N_2. As has also been pointed out by Terao [2], an ordering of vacancies leads to a different unit cell. The structure of β-Ta_2N (which was called γ-Ta_2N by Terao [2]) is then trigonal, with space group $P\bar{3}1m$. The cell can then be chosen as described by Terao [2] in his Fig. 11, which has been discussed and confirmed by Conroy and Christensen [14]. The unit cell then has an a-lattice parameter of 5.28 Å. A comparison of the stability of hexagonal ($P\frac{6}{m}mm$) and cubic TaN, based on the enthalpy of formation derived from DFT LDA-calculations has recently been given by Violet et al. [18]. In that study, stoichiometric cubic δ-TaN was significantly more stable than the hexagonal $P\frac{6}{m}mm$-polymorph. However, as has been mentioned above, the $P\frac{6}{m}mm$-polymorph has long been discredited [4], and the hexagonal stoichiometric ground state structure of ε-TaN has $P\bar{6}2m$-symmetry. Kroll et al. [19] predicted that a novel Ta_3N_5-II polymorph could by synthesized from the mononitride at pressures above 17–25 GPa at 2800 K, while a transformation from Ta_3N_5-I to Ta_3N_5-II was thought to occur at 9 GPa. Recently, Jiang et al. [20] found from DFT calculations that the new orthorhombic high-pressure phase η-Ta_2N_3 is mechanically unstable because of a negative c_{66} elastic constant. They suggested that minor oxygen substitution for nitrogen stabilizes this structure.

From this summary of previous work, a number of questions remain. We address here in which sequence and what phases appear at high-(P, T) conditions in diamond anvil cell based experiments, where nitrogen is present in excess. This is investigated by an in situ observation of the reaction of tantalum with nitrogen in a laser heated diamond anvil cell. The synthesis of nitrides in laser-heated diamond anvil cells has already been explored earlier (see review by Horvath-Bordon et al. [21]). For example, a number of transition metal nitrides were synthesized in a laser-heated DAC at ≈ 10 GPa and ≈ 1800 K and the recovered samples were analysed ex situ [22], but in that study, the synthesis of tantalum nitride has not been attempted. Further examples for in situ syntheses of binary transition metal nitrides include those of c-Hf_3N_4 and c-Zr_3N_4 [23], cubic PtN_2 [24,25], trigonal IrN_2 [25,26], and orthorhombic OsN_2 [26]. Also, the bulk modulus of cubic δ-TaN has not been determined experimentally yet, nor that of orthorhombic η-Ta_2N_3, and theoretical values, obtained from density functional theory calculations, range from 329 to 372 GPa for δ-TaN [27]. Further, we revisit the question of the relative stability of ε-TaN to δ-TaN and study the possibility of transition into $Pm\bar{3}m$-TaN by parameter-free density functional theory based calculations. This was thought to be interesting, as B1 (NaCl) type structures often transform into B2 (CsCl) type structures on pressure increase [28].

2. Experimental

Small pieces of tantalum foil (Alfa Aesar No. 10351, purity 99.95%) with an initial thickness of 25 μm served as starting material. The foils were thinned to <5–10 μm thickness while cutting plates with horizontal dimensions of about 30–80 μm. The pieces were loaded into Boehler–Almax diamond anvil cells, DACs, with conical anvils and 0.35 mm culets and effective apertures of ≈ 48° and 60°, which were used for pressure generation [29]. Tungsten was used as the gasket material, preindented to 40–45 μm. Gasket holes with a diameter between 130 and 190 μm were drilled by a home-built laser lathe. For the thermal isolation of tantalum from the diamond anvil different materials were used in order to check for a reaction with the isolating layer. We used thin layers of compressed powder of sodium chloride (exp. 5 and 6, Table 2), magnesium oxide (exp. 2 and 3), and aluminium oxide (exp. 4), and single-crystalline sapphire chips of 5 μm thickness (exp. 1) on top of one or both anvils. Small pieces of ruby were loaded for pressure determination. Liquid nitrogen was loaded at a pressure of 0.18 GPa within a pressure vessel as both a reaction component and a pressure transmitting medium.

Experiments were conducted ex situ in house with a 100 W fiber laser (1.07 μm wavelength) or a 250 W CO_2 laser (10.6 μm wavelength), and in situ at beamline

Table 2
Overview of the experiments. In all the experiments a piece of tantalum foil was loaded together with nitrogen as pressure-transmitting medium and reactant, and with rubies for pressure determination. In situ X-ray diffraction measurements at high pressure, before, during, and after laser heating were performed at ALS, ex situ laser heating in Frankfurt.

No.	Type	Isolation	P_{max}/GPa	Laser, power$_{max}$	Final reaction products
1	In situ	Al_2O_3 crystal, sandwich	26.0(1)	2 fiber, 16 W	η-Ta_2N_3
2	In situ	MgO powder, single layer	27.0(2)	2 fiber, 16 W	η-Ta_2N_3+unknown phase
3	Ex situ	MgO powder, single layer	9(1)	CO_2, 20 W	TaN_x+β-Ta_2N+η-Ta_2N_3+unknown phase
4	Ex situ	Al_2O_3, powder, single layer	11(1)	Yb fiber, 8 W	η-Ta_2N_3
5	Ex situ	NaCl powder, sandwich	11.5(5)	Yb fiber, 9 W	η-Ta_2N_3
6	Ex situ	NaCl powder, single layer	14.1(1)	Yb fiber, 9 W	η-Ta_2N_3

12.2.2. at the Advanced Light Source (ALS, Berkeley, USA) (Table 2). The four samples heated in house at 9(1), 11(1), 11.5(5), and 14.1(1) GPa were recovered from the diamond anvil cell and measured at the ALS for identification of the reaction products. For the experiments at the ALS we used 25 and 30 keV synchrotron X-ray radiation and double-sided laser heating with two 100 W fiber lasers (1.09 μm wavelength). The experimental set-up is described in detail in Caldwell et al. [30]. Tantalum and the tantalum nitride reaction products were laser heated from one or both sides at different laser power (temperature) up to a total of 16 W with the fiber lasers. There was little absorption of the CO_2 laser radiation (10.6 μm) by tantalum within the nitrogen medium and high laser power resulted in only weak hot spots (exp. 3, Table 2), the fiber laser radiation (1.07–1.09 μm) was strongly absorbed by the opaque tantalum and only moderate laser power was required to achieve bright hot spots. However, due to technical problems, the determination of the temperature was problematic during the experiments, and hence only a very rough estimate of the temperature was obtained from visual observation. Powder diffraction images were collected with a MAR345 online image-plate scanner. The sample-to-detector distances of 309.80 and 346.80 mm, respectively, were determined from a LaB_6-reference sample. Counting times varied between 120 and 720 s. Most data collection was done with a 10 μm × 10 μm beam spot. The laser spots had diameters of about 30 μm. The diffraction images were processed and integrated using FIT2D [31]. Intense and well-defined single-crystal diffraction spots from individual larger grains of the sample as well as scattering from the carbon mirrors during laser heating were masked manually and excluded from the integration. The background of the integrated powder diffraction patterns was extracted using the program DATLAB [32]. Le Bail fits and Rietveld fits with constrained structural models were performed using the program GSAS (General Structure Analysis System) [33] in order to obtain unit cell parameters. The background was interpolated between several manually selected points and a shifted Chebyshev function was used. Pressures were determined with an off-line spectrometer at ambient temperature using the ruby-fluorescence method [34]. In situ diffraction data were collected from two samples at ambient temperature prior and after laser heating (at 9.8(7) and 26.1(2) GPa in exp. 1, and at 12.7(5), 19.7(3), and 27.0(2) GPa in exp. 2, Table 2), at different positions on the samples, and in steps on pressure increase and decrease. The final reaction products were further analysed at ambient pressure within the diamond anvil cell and also after recovering them from the DAC.

3. Computational details

Density functional theory calculations have extensively been used to model structure–property relations of transition metal carbides and nitrides. Here, we use the CASTEP program [35–37], which employs a plane wave basis set in conjunction with ultrasoft pseudopotentials. The plane-wave basis set is unbiased (as it is not atom-centred) and does not suffer from the problem of basis-set superposition error (BSSE) unlike atom-centred basis sets. It also makes converged results straightforward to obtain in practice as the convergence is controlled by a few adjustable parameters. The PBE [38] exchange-correlation functional was employed in the calculations.

Geometry optimisations were performed with the CASTEP code using pseudopotentials from the CASTEP database. Plane-wave cutoff of 330 eV was used, and Brillouin–Zone integrals were performed using Monkhorst–Pack grids [39] with spacings between grid points of ≤ 0.03 Å^{-1}. Concurrent geometry optimisation of the unit cell and internal co-ordinates was performed so that forces were converged to 0.005 eV/Å and stress residuals to 0.005 GPa.

The tantalum pseudopotential was tested by computing the lattice parameter ($a_{theo} = 3.296$ Å, $a_{exp} = 3.301$ Å) and the bulk modulus ($B_{0,theo} = 223$ GPa, $B_{0,exp} = 196$ GPa [40]).

4. Results

4.1. Phase stability

The image recorded with an image plate obtained before any heating and the corresponding powder diffraction pattern of experiment 1 (Table 2) are shown in Fig. 1. Essentially all reflections could be indexed by an assignment of peaks to either Ta, W (from the gasket) or δ-N_2. Refined lattice parameters are given in Table 3.

A short irradiation with the laser beams during laser alignment (2 W each laser) showing a weak hot spot triggered a reaction (exp. 1). The image and diffraction pattern are shown in Fig. 1. While the strong powder rings, which still show the same texture like before, can be indexed with the tantalum structure ($Im\bar{3}m$), the obtained unit cell parameter is definitely larger than before laser heating (Table 3). This can be attributed to the incorporation of small amounts of nitrogen into tantalum. Already Schönberg [41] has reported the incorporation of nitrogen in tantalum forming non-stoichiometric $TaN_{0.05}$ with an expanded lattice parameter of 3.369 Å compared to that of pure tantalum with 3.311 Å [41]. This was confirmed by the nitrogen–tantalum phase diagram showing the formation of TaN_x with x up to 0.15 at high temperatures (<3200 K) and of Ta_2N and TaN on successive nitridation ([42,43] cited in [1]). Hence, we conclude that the phase observed here shows the starting nitridation process at high pressure and increased temperature and that the nitrogen content of this phase should be not more than about 15 atomic %.

The formation of this phase was also confirmed in experiments number 2 and 3 (Table 2), where additionally to the major component of cubic ($Im\bar{3}m$) TaN_x, hexagonal β-Ta_2N and small amounts of the orthorhombic high-pressure phase η-Ta_2N_3 as described by Zerr et al. [12] were present (Fig. 2). The laser power of the in situ experiment 2 was ≈8 W (4 W each laser) at 12.7(5) GPa. Experiment 3 was performed ex situ using the CO_2 laser, which was only weakly absorbed by tantalum in nitrogen medium at 9(1) GPa and resulted in the same three tantalum nitride phases, which were confirmed from a measurement of the recovered sample. This shows that on further temperature increase at pressures between about 9 and 13 GPa a further nitridation of TaN_x to β-Ta_2N and η-Ta_2N_3 takes place. The reaction products might be non-stoichiometric, the compositional range, however, was not further investigated here.

Successive laser heating at higher power (up to 16 W, 8 W each laser) led to the formation of a pure η-Ta_2N_3 phase in experiments 1, 4, 5, and 6 (Fig. 1, Table 2). Again, the investigation of the degree of stoichiometry was not a matter of this study. All the tantalum reacted immediately in all steps of nitridation, pure tantalum was not present any more in either of the samples. A reaction of the tantalum foil can easily be confirmed visually using a microscope due to the loss of the metallic luster of the sample surface. η-Ta_2N_3 remained stable on pressure increase to 20, 26 and 27 GPa and further laser heating at these pressures, and on pressure decrease down to ambient conditions (exp. 1 and 2). We conclude, that η-Ta_2N_3 is the stable tantalum nitride high-pressure phase on

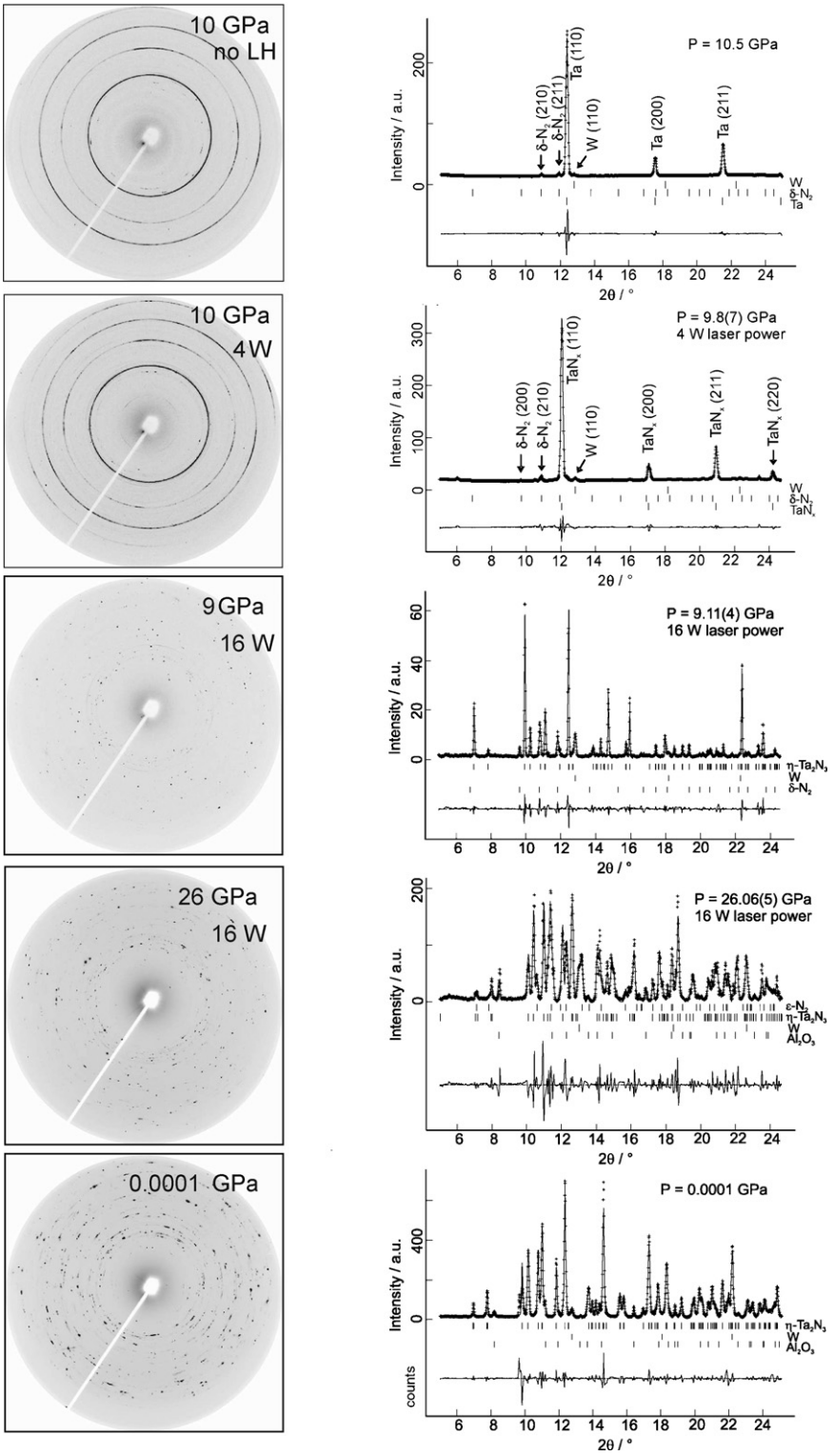

Fig. 1. Image plate frames (left) and corresponding refined powder X-ray diffraction patterns (right) from top to bottom for the unreacted tantalum foil at 10.5 GPa (λ = 0.4958 Å), the TaN_x after short laser alignment with a total of 4 W laser power, the fully reacted η-Ta_2N_3 after strong laser heating with a total power between 6 and 16 W at 9 and 26 GPa, respectively, and the recovered sample at ambient conditions (experiment 1). On pressure increase the gasket hole was decreased and the isolating single-crystalline sapphire chip was broken, hence accounting for the diffraction lines of Al_2O_3 at 26 GPa and in the recovered sample. Right: Symbols (+) represent experimental values. The result of the Rietveld fit is shown by the continuous line through the data points. Vertical bars show the positions of the allowed Bragg reflections of the different phases. The difference curve is plotted below.

nitrogen excess at pressures between 9 and 27 GPa and temperatures up to at least 1600–2000 K. With our experiments we have shown in situ the synthesis of this phase for the first time and confirmed its high-(P,T)-stability as was already assumed previously by Zerr et al. [12], who discovered this phase as a quench product from ex situ multi anvil press syntheses.

From our experiments using different isolating layers during DAC loading we can exclude a reaction of tantalum and nitro-

Table 3
Selected refined cell parameters of starting and reaction products before and after laser heating (experiment 1).

Compound	Space group	a /Å	b /Å	c /Å
Starting material at 9.8(7) GPa				
Ta	$Im\bar{3}m$	3.24842(8)		
W	$Fm\bar{3}m$	3.14 (fixed)		
δ-N_2	$Pm\bar{3}n$	5.839 (fixed)		
Reaction products after laser alignment at 4 W at 9.8(7) GPa				
TaN_x	$Im\bar{3}m$	3.3426(2)		
W	$Fm\bar{3}m$	3.14 (fixed)		
δ-N_2	$Pm\bar{3}n$	5.839 (fixed)		
Reaction products after laser heating at 16 W at 9.11(4) GPa				
η-Ta_2N_3	$Pbnm$	8.0904(4)	8.1156(5)	2.9511(1)
W	$Fm\bar{3}m$	3.1415(6)		
δ-N_2	$Pm\bar{3}n$	5.9 (fixed)		
Sample after laser heating at 16 W at 26.06(5) GPa				
η-Ta_2N_3	$Pbnm$	7.917(1)	8.032(1)	2.9163(4)
W	$Fm\bar{3}m$	3.0934(8)		
$(Al,Cr)_2O_3$	$R\bar{3}c$	4.6308(7)		12.607(4)
ϵ-N_2	$R\bar{3}c$	7.266(2)		10.325(9)
Sample at ambient conditions				
η-Ta_2N_3	$Pbnm$	8.1474(8)	8.1804(8)	2.9683(2)
W	$Fm\bar{3}m$	3.1520(6)		
$(Al,Cr)_2O_3$	$R\bar{3}c$	4.757(1)		12.890(7)

Table 4
Bulk moduli B_0 obtained from fits of 2nd- and 3rd-order Birch-Murnaghan equations of state to the experimental and theoretical data of η-Ta_2N_3.

	V_0/Å^3	B_0/GPa	B'
Exp-2nd-order	199.5(2)	319(6)	4 (fixed)
Exp-3rd-order	199.6(2)	311(6)	4.67 (fixed)
DFT-2nd-order	206.36(2)	348.0(9)	4
DFT-3rd-order	206.42(1)	339(1)	4.67(9)
	a_0/Å	B_{a0}/GPa	B'_a
Exp-2nd-order	8.190(8)	239(13)	4
DFT-2nd-order	8.2492(4)	239.6(6)	4
DFT-3rd-order	8.2488(5)	242(2)	3.8(2)
	b_0/Å	B_{b0}/GPa	B'_b
Exp-2nd-order	8.198(4)	342(13)	4
DFT-2nd-order	8.3067(5)	500(3)	4
DFT-3rd-order	8.3079(2)	471(3)	6.2(2)
	c_0/Å	B_{c0}/GPa	B'_c
Exp-2nd-order	2.977(1)	348(8)	4
DFT-2nd-order	3.01192(8)	391.2(9)	4
DFT-3rd-order	3.01211(6)	383(2)	4.6(1)

gen with NaCl (at 11–14 GPa and on laser heating, exp. 5 and 6, Table 2) and with Al_2O_3 (exp. 1 and 4), where tantalum was double-sandwiched and in close contact with these layers. However, we cannot exclude a reaction with MgO (exp. 2 and 3), as these in situ and ex situ experiments showed the appearance of an unidentified additional phase (Fig. 2). When heating the in situ sample of experiment 2 at 27 GPa with 16 W laser power, strong peaks of another phase appeared in addition to the η-Ta_2N_3 phase. Whether these unidentifed phases are due to a reaction with MgO or due to impurities in MgO cannot be resolved from our data. However, it can be excluded due to the results of the other experiments, that this additional phase is a pure tantalum nitride.

4.2. Bulk and linear compressibility

Results from least-squares fits of 2nd- and 3rd-order Birch–Murnaghan equations of state (BM-EOS) to the pressure–volume (P–V) data and the pressure dependencies of the individual cell axes using the program EOS-FIT [44] are summarised in Table 4 and plotted in Fig. 3. Due to the heating process at different pressures, the experimental data scatter significantly. Hence, they were fitted with 2nd-order BM-EOS using unit weights or 3rd-order BM-EOS and B' fixed to the values obtained from fits to the DFT results, while the DFT results were fitted with both, 2nd- and 3rd-order BM-EOS.

The predicted unit cell parameters of η-Ta_2N_3 at 0 GPa are larger by <1.5% compared to the experiment, which is often observed in DFT-GGA calculations such as those performed here. The bulk modulus B_0 determined experimentally in this study is smaller by ≈ 9% than the bulk modulus obtained from a BM-EOS fit to the DFT results (Table 4).

The linear compressibilities of η-Ta_2N_3 are anisotropic (Table 4). As the unit cell shows a pseudo-tetragonal metric with the a axis being slightly larger than the b axis according to Zerr et al. [12], an unambiguous assignment of these axes was not possible from our high-pressure data. Further, we cannot exclude a possible cross-over of the experimental values, such that $b > a$ at high pressure. In the relaxed theoretical geometry the a axis is shorter than the b axis. Our experimental and theoretical data are consistent in that the shorter of these axes is more compressible (Table 4). As the

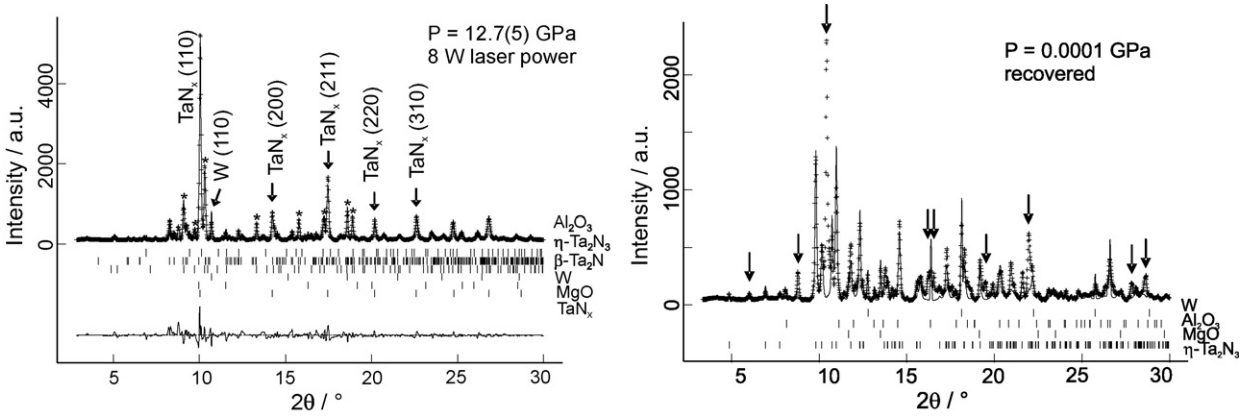

Fig. 2. Refined powder X-ray diffraction patterns for another reacted tantalum sample (experiment 2). Left: After laser alignment with 8 W at 12.7(5) GPa the formation of TaN_x, β-Ta_2N (reflections marked by stars) and a small amount of η-Ta_2N_3 was observed (λ = 0.4132 Å). Right: The recovered sample after subsequent laser heating at 16 W at 27 GPa shows an unidentified phase (reflections marked by arrows) in addition to η-Ta_2N_3, which might be a reaction product with MgO (λ = 0.4958 Å). Symbols (+) represent experimental values. The result of the LeBail fit is shown by the continuous line through the data points. Vertical bars show the positions of the allowed Bragg reflections of the different phases, which are assigned from top to bottom on the right. The difference curve is plotted below (left).

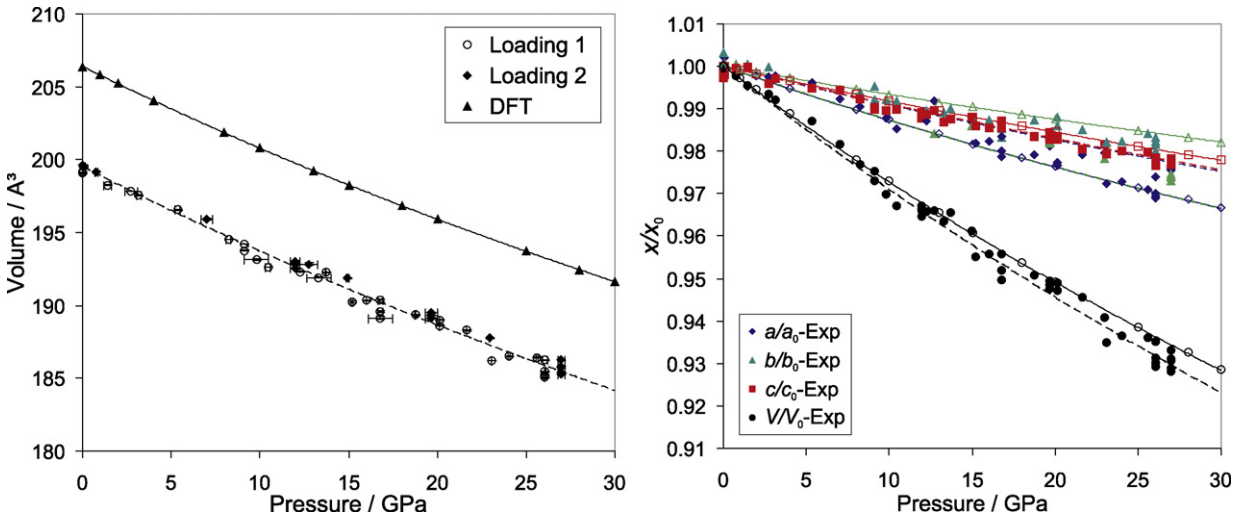

Fig. 3. Pressure dependence of the η-Ta_2N_3 unit cell volume (left) and of the normalised unit cell parameters (right, colour online). Dashed and solid lines represent BM-EOS fits to the experimental and theoretical results, respectively. Right: DFT data are plotted with open symbols.

compression mechanism of the structural model is plausible (see next section), we assume that the assignment of the linear compressibilities is correct in the DFT model and that the *a* axis is the most compressible axis with $B_{a0} < B_{c0} < B_{b0}$ from model calculations and $B_{a0} < B_{b0} \approx B_{c0}$ from experiment. This is also consistent with the theoretical results by Jiang et al. [20]. They obtained a smaller value for the *a* axis as well, which further is softer than the *b* axis as derived from the elastic constants. The present data therefore disagree with the assignment of Zerr et al. [12], and instead we currently prefer the assignment given in Tables 3 and 4 and Fig. 3.

4.3. Structural compression from DFT

The structural parameters of the relaxed structures are in good agreement with experimental data (Table 1). The lattice parameters agree within 2.5%, and the *c*/*a*-ratios are reproduced with 0.7% for all tantalum nitrides investigated here. Hence, we predict the compression behaviour of η-Ta_2N_3.

The crystal structure of η-Ta_2N_3 is of the orthorhombic U_2S_3-structure type (*Pbnm*) and consists of a network of edge-sharing Ta(1)N_7 and Ta(2)N_{7+1} polyhedra (Fig. 4). Due to the edge-sharing, the crystal structure is very incompressible and the main compression is achieved via compression of the bond distances. The anisotropy of the linear compressibilities can be explained by the orientation of the longest Ta–N bond of the Ta(2)N_{7+1} polyhedron, which is 2.599 Å compared to 2.124–2.238 Å for the other Ta–N bond distances. This longest bond is nearly parallel to the *a* axis and is compressed most at increasing pressure, which is responsible for the larger compressibility of the *a* axis (Fig. 4). The compression of this bond is accompanied by an increase of the Ta(1)–N(3)–Ta(1) and Ta(1)–N(2)–Ta(2) angles by ≈ 2.4° and ≈ 2.2°, respectively, between 0 and 30 GPa, and a slight decrease of the N(2)–Ta(1)–N(3) angle by ≈ 1.7° (Fig. 4). All the other inter- and intra-polyhedral angles change by <1.4°. The Ta(1)–N(3)–Ta(1) angle is oriented nearly parallel to the *b* axis, hence accounting for the large incompressibility of this axis.

We also computed the relative stabilities of the mononitrides as a function of pressure, in order to test if the B2 structure would become stable on increasing pressure. We find that at ambient pressure the ε- and ϑ-phase have equal total energies, and that the δ- and the B2-phase are significantly less stable. Pressure stabilises the ϑ-phase in relation to all other phases, and at 50 GPa the ϑ-phase is more stable than the other mononitrides by 50–100 kJ/mol.

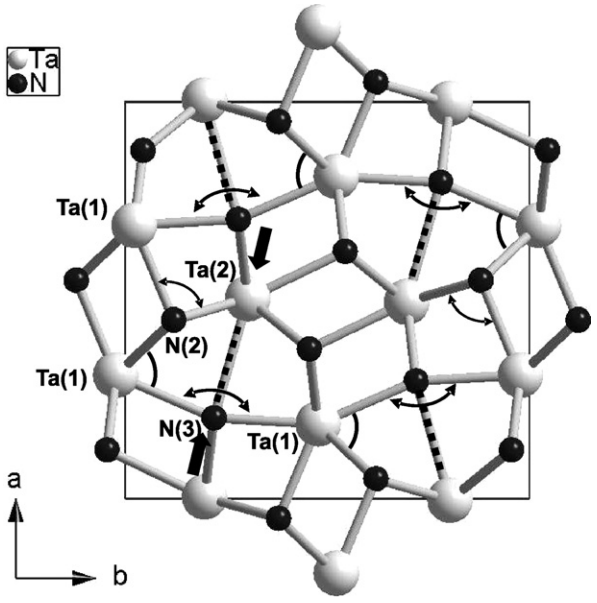

Fig. 4. Crystal structure of η-Ta_2N_3 at 0 GPa from DFT. The compression of the long Ta(2)–N(3) bonds parallel to the *a* axis (dashed lines) is indicated by the bold arrows. The pressure-induced increases of the Ta(1)–N(3)–Ta(1) angle parallel to the *b* axis and of the Ta(1)–N(2)–Ta(2) angle are shown by the thin arrows. The N(2)–Ta(1)–N(3) angle is indicated by a circular arc.

5. Discussion

We have shown by experiment the occurrence of a sequence of reactions during laser heating tantalum embedded in nitrogen within the diamond anvil cell at high pressures (up to 27 GPa) and temperatures (>1600–2000 K, up to 16 W laser power). The nitridation sequence of tantalum at high pressure and temperature commences with the direct formation of TaN_x ($Im\bar{3}m$) upon short double-sided laser heating with a total laser power of 4 W (each laser 2 W) resulting in weak hot spots, as derived from a moderate, but significant, enlargement of the unit cell. Hence, the activation energy for this reaction seems to be small at elevated pressure. TaN_x has been reported in a range of non-stoichiometric compositions up to $x = 0.15$ with a cell parameter of 3.369 Å for $x \approx 0.05$ [41]. The cell parameter refined at ambient conditions from the sample of experiment 3 (Table 2), which was recov-

ered after CO_2-laser heating at 9(1) GPa, is slightly larger with $a = 3.39(1)$ Å, which is supposed to be related to a higher nitrogen content ($0.05 < x < 0.15$) from nitridation at high pressure and temperature. Assuming a linear correlation between the nitrogen content and the lattice parameter, x would be ≈ 0.07 in our experiments. Neglecting the influence of pressure, this would correspond to a synthesis temperature of about 1770 K ([42,43] cited in [1]). The sample of experiment 2 shows $a = 3.334(1)$ Å at 12.7(5) GPa after double-sided laser heating with a total of 8 W (Fig. 2). Pure tantalum has a lattice parameter of 3.24 Å at this pressure applying the equation of state from Dewaele et al. [45]. Hence, $x \approx 0.08$ for this TaN_x phase.

We have not observed the formation of ε-TaN nor of the high-pressure phase δ-TaN in our experiments. This result implies, that δ-TaN is obtained from hexagonal ε-TaN, which is the stable phase at room conditions, but not from a direct reaction of the elements at elevated P, T-conditions. This is an important result with respect to the exploration of new synthesis routes for tantalum nitrides.

The successive disappearance of cubic TaN_x on further laser heating at increasing temperature is associated with further reactions with excess nitrogen. The increasing nitrogen content leads to the formation of β-Ta_2N in a next step and of η-Ta_2N_3 as the final reaction product and stable high-P, T phase. The composition of both phases might differ from stoichiometry. Further nitridation is not observed. In our experiments at elevated P, T-conditions (up to 27 GPa, >1600–2000 K) we did not observe the formation of Ta_3N_5-I or a novel Ta_3N_5-II phase. A Ta_3N_5-II phase was predicted to be synthesized from ε-TaN at pressures above 17–25 GPa at 2800 K [19]. Nor did we observe the tetragonal Ta_2N_3 phase during synthesis or on pressure release, which was predicted to be the stable phase below 7 GPa by Jiang et al. [20].

A comparison of the experimentally obtained bulk modulus of η-Ta_2N_3 ($B_0 = 319(6)$ GPa) with the bulk modulus obtained from elastic constants calculated from DFT results by Jiang et al. [20] ($B_0 = 327$ GPa) and calculated from the structural compression ($B_0 = 323$ GPa) shows very good agreement. The oxygen substitution of nitrogen in $Ta_{16}N_{22}O_2$ as proposed by Jiang et al. [20] would result in a slightly larger compressibility with a B_0 even closer to our experimental value.

The results further show that η-Ta_2N_3 is much less compressible than pure tantalum with $B_0 = 194$ GPa [45]. It is also less compressible than δ-HfN, δ-ZrN, and the cubic high-pressure nitrides c-Hf_3N_4 and c-Zr_3N_4 (with bulk moduli 260 GPa, 248 GPa, 241 GPa and 250 GPa, respectively [46,47,23]), however, more compressible than the transition metal nitrides δ-MoN, δ-NbN, PtN_2, OsN_2, or IrN_2 (with bulk moduli 345 GPa, 348 GPa, 372 GPa, 358 GPa and 428 GPa, respectively [48,46,24,26]) or than c-BN (369 GPa [49]). In comparison to transition metal carbides, η-Ta_2N_3 is less or similar compressible than ZrC, HfC, NbC or TiC (207 GPa, 241 GPa, 296 GPa and 315 GPa, respectively [1]); and more compressible than VC, Re_2C, TaC or WC (390 GPa, 405 GPa, 414 GPa and 421 GPa, respectively [1,50]).

6. Conclusions

Three reaction products were observed for tantalum and nitrogen in the laser-heated diamond anvil cell as a function of laser power (temperature). In a first step cubic TaN_x with $0.05 < x < 0.10$ was formed. In a second step on further reaction with nitrogen additional, nitrogen-enriched β-Ta_2N was observed. The final reaction product at high-P, T was η-Ta_2N_3 as a pure and stable phase. This high-P, T polymorph is rather incompressible with a bulk modulus $B_0 \approx 319$ GPa. We plan further experiments in the laser-heated diamond anvil cell using ε-TaN as starting material (1) without and (2) with nitrogen excess in the pressure chamber in order to answer the question, whether δ-TaN or η-Ta_2N_3 are the stable high-P, T tantalum nitrides under these preconditions. Further, the lower P, T-limit for synthesis of the η-Ta_2N_3 phase will be explored.

Acknowledgements

This research was supported by Deutsche Forschungsgemeinschaft (projects WI-1232/25-1, WI-1232/26-1, FR2491/2-1) in the framework of the DFG-SPP 1236, and by the BMBF (project 05KS7RF1). AF thanks the CNV-foundation and the FOKUS program of the Goethe-university for financial support. The Advanced Light Source is supported by the Director, Office of Science, Office of Basic Energy Sciences, of the U.S. Department of Energy under Contract No. DE-AC02-05CH11231. This research was partially supported by COMPRES, the Consortium for Materials Properties Research in Earth Sciences under NSF Cooperative Agreement EAR 06-49658, by the Goethe-university Frankfurt, and by the Vereinigung der Freunde und Förderer der Goethe-Universität.

References

[1] H.O. Pierson, Handbook of Refractory Carbides and Nitrides, Noyes Publication, 1996.
[2] N. Terao, Japanese Journal of Applied Physics 10 (1971) 248–259.
[3] J. Gatterer, G. Dufek, P. Ettmayer, H. Kieffer, Monatshefte für Chemie 106 (1975) 1137–1147.
[4] A.N. Christensen, B. Lebech, Acta Crystallographica B 34 (1978) 261–263.
[5] G. Brauer, K.H. Zapp, Die Naturwissenschaften 40 (1953) 604.
[6] G. Brauer, K.H. Zapp, Zeitschrift für anorganische und allgemeine Chemie 277 (1954) 129–139.
[7] L.G. Boiko, S.V. Popova, JETP Letters USSR 12 (1970) 70–71.
[8] G. Brauer, E. Mohr, A. Neuhaus, A. Skokan, Monatshefte für Chemie 103 (1972) 794–798.
[9] T. Mashimo, S. Tashiro, T. Toya, M. Nishida, H. Yamazaki, S. Yamaya, K. Oh-Ishi, S. Syono, Journal of Materials Science 28 (1993) 3439–3443.
[10] E. Gillan, R.B. Kaner, Inorganic Chemistry 33 (1994) 5693–5700.
[11] W. Ensinger, M. Kiuchi, M. Satou, Journal of Applied Physics 77 (1995) 6630–6635.
[12] A. Zerr, G. Miehe, J. Li, D.A. Dzivenko, V.K. Bulatov, H. Höfer, N. Bolfan-Casanova, M. Fialin, G. Brey, T. Watanabe, M. Yoshimura, Advanced Functional Materials 19 (2009) 2282–2288.
[13] A. Fontbonne, J.C. Gilles, Revue International des haute Temperatures et des Refractaires 6 (1969) 181.
[14] L.E. Conroy, A.N. Christensen, Journal of Solid State Chemistry 20 (1977) 205–207.
[15] J. Strähle, Zeitschrift für allgemeine und anorganische Chemie 402 (1973) 47–57.
[16] N.E. Brese, M. O'Keefe, P. Rauch, F.J. DiSalvo, Acta Crystallographica C47 (1991) 2291–2294.
[17] C. Stampfl, A.J. Freeman, Physical Review B 71 (2005) 02411.
[18] P. Violet, E. Blanquet, O. Le Bacq, Microelectronic Engineering 83 (2006) 2077–2081.
[19] P. Kroll, T. Schröter, M. Peters, Angewandte Chemie—International edition 44 (2005) 4249–4254.
[20] C. Jiang, Z. Lin, Y. Zhao, Physical Review Letters 103 (2009) 185501.
[21] E. Horvath-Bordon, R. Riedel, A. Zerr, P.F. McMillan, G. Auffermann, Y. Prots, W. Bronger, R. Kniep, P. Kroll, Chemical Society Reviews 35 (2006) 987–1014.
[22] M. Hasegawa, T. Yagi, Journal of Alloys and Compounds 403 (2005) 131–142.
[23] A. Zerr, G. Miehe, R. Riedel, Nature Materials 2 (2003) 185–189.
[24] E. Gregoryanz, C. Sanloup, M. Somayazulu, J. Badro, G. Fiquet, H.-k. Mao, R.J. Hemley, Nature Materials 3 (2004) 294–297.
[25] J.C. Crowhurst, A.F. Goncharov, B. Sadigh, C.L. Evans, P.G. Morrall, J.L. Ferreira, A.J. Nelson, Science 311 (2006) 1275–1278.
[26] A.F. Young, C. Sanloup, E. Gregoryanz, S. Scandolo, R.J. Hemley, H.-k. Mao, Physical Review Letters 96 (2006) 155501.
[27] E.I. Isaev, S.I. Simak, I.A. Abrikosov, R. Ahuja, Y.K. Vekilov, M.I. Katsnelson, A.I. Lichtenstein, B. Johansson, Journal of Applied Physics 101 (2007), Art. No. 123519.
[28] P. Toledano, K. Knorr, L. Ehm, W. Depmeier, Physical Review B 67 (2003), Art. No. 144106.
[29] R. Boehler, Review of Scientific Instruments 77 (2006) 115103.
[30] W. Caldwell, M. Kunz, R. Celestre, E.E. Domning, M.J. Walter, D. Walker, J. Glossinger, A.A. MacDowell, H.A. Padmore, R. Jeanloz, S.M. Clark, Nuclear Instruments and Methods in Physics Research A 582 (2007) 221–225.
[31] A.P. Hammersley, S.O. Svensson, M. Hanfland, A.N. Fitch, D. Hausermann, High Pressure Research 14 (1996) 235–248.
[32] K. Syassen, DATLAB. Version 1.37d, MPI/FKF Stuttgart, Germany, 2005.

[33] A.C. Larson, R.B. Von Dreele, Los Alamos National Laboratory Report LAUR (1994) 86–748.
[34] H. Mao, P. Bell, J. Shaner, D. Steinberg, Journal of Applied Physics 49 (1978) 3276–3283.
[35] M.D. Segall, P.J.D. Lindan, M.J. Probert, C.J. Pickard, P.J. Hasnip, S.J. Clark, M.C. Payne, Journal of Physics: Condensed Matter 14 (2002) 2717–2744.
[36] S.J. Clark, M.D. Segall, C.J. Pickard, P.J. Hasnip, M.J. Probert, K. Refson, M.C. Payne, Zeitschrift für Kristallographie 220 (2005) 567–570.
[37] K. Refson, P.R. Tulip, S.J. Clark, Physical Review B 73 (2006) 155114.
[38] J.P. Perdew, K. Burke, M. Ernzerhof, Physical Review Letters 77 (1996) 3865–3868.
[39] H.J. Monkhorst, J.D. Pack, Physical Review B 13 (1976) 5188–5192.
[40] H. Wern, Single Crystal Elastic Constants and Calculated Bulk Properties: A Handbook, Logos Verlag Berlin, 2004.
[41] N. Schönberg, Acta Chemica Scandinavica 8 (1954) 199–203.
[42] W.G. Moffatt, The Handbook of Binary Phase Diagrams, Genum Publishing Corp, Schenectady, NY, 1984.
[43] T.B. Massalski, Binary Alloy Phase Diagrams, 2nd edition, ASM International, Metals Park, OH, 1990.
[44] R. Angel, EOS-FIT, 1998. Version 4.2.
[45] A. Dewaele, P. Loubeyre, M. Mezouar, Physical Review B 69 (2004) 092106.
[46] X.-J. Chen, V.V. Struzhkin, Z. Wu, M. Somayazulu, J. Qian, S. Kung, A.N. Christensen, Y. Zhao, R.E. Cohen, H.-k. Mao, R.J. Hemley, Proceedings of the National Academy of Sciences of the United States of America 102 (2005) 3198–3201.
[47] D.A. Dzivenko, A. Zerr, R. Boehler, R. Riedel, Solid State Communications 139 (2006) 255–258.
[48] E. Soignard, P.F. McMillan, T.D. Chaplin, S.M. Farag, C.L. Bull, M.S. Somayazulu, K. Leinenweber, Physical Review B 68 (2003) 132101.
[49] E. Knittle, R.M. Wentzcovitch, R. Jeanloz, M.L. Cohen, Nature 337 (1989) 349–352.
[50] E.A. Juarez-Arellano, B. Winkler, A. Friedrich, L. Bayarjargal, V. Milman, J. Yan, S.M. Clark, Journal of Alloys and Compounds 481 (2009) 577–581.